AGU PUBLICATIONS

JGR

Journal of Geophysical Research: Space Physics

RESEARCH ARTICLE

10.1002/2017JA024221

Key Points:
- A complete corotation electric field model has been derived from magnetic measurements of the Swarm satellite mission
- The equations of the global corotation electric field and secondary corotation charges are given in corotating and inertial coordinates
- An accurate corotation electric field model is essential for the understanding of plasmasphere underrotation and other phenomena

Correspondence to:
S. Maus,
stefan.maus@colorado.edu

Citation:
Maus, S. (2017), A corotation electric field model of the Earth derived from Swarm satellite magnetic field measurements, *J. Geophys. Res. Space Physics*, *122*, 8733–8754, doi:10.1002/2017JA024221.

Received 1 APR 2017
Accepted 16 JUL 2017
Accepted article online 25 JUL 2017
Published online 3 AUG 2017
Corrected 14 SEP 2017

This article was corrected on 14 SEP 2017. See the end of the full text for details.

A corotation electric field model of the Earth derived from Swarm satellite magnetic field measurements

Stefan Maus[1]

[1]CIRES, University of Colorado Boulder, Boulder, Colorado, USA

Abstract Rotation of the Earth in its own geomagnetic field sets up a primary corotation electric field, compensated by a secondary electric field of induced electrical charges. For the geomagnetic field measured by the Swarm constellation of satellites, a derivation of the global corotation electric field inside and outside of the corotation region is provided here, in both inertial and corotating reference frames. The Earth is assumed an electrical conductor, the lower atmosphere an insulator, followed by the corotating ionospheric *E* region again as a conductor. Outside of the Earth's core, the induced charge is immediately accessible from the spherical harmonic Gauss coefficients of the geomagnetic field. The charge density is positive at high northern and southern latitudes, negative at midlatitudes, and increases strongly toward the Earth's center. Small vertical electric fields of about 0.3 mV/m in the insulating atmospheric gap are caused by the corotation charges located in the ionosphere above and the Earth below. The corotation charges also flow outward into the region of closed magnetic field lines, forcing the plasmasphere to corotate. The electric field of the corotation charges further extends outside of the corotating regions, contributing radial outward electric fields of about 10 mV/m in the northern and southern polar caps. Depending on how the magnetosphere responds to these fields, the Earth may carry a net electric charge.

1. Introduction

A series of magnetic satellites, from the past Ørsted [*Thomsen and Hansen*, 1999] and CHAMP [*Reigber et al.*, 2002] to the ongoing Swarm mission [*Friis-Christensen et al.*, 2006], has enabled mapping of the geomagnetic field in unprecedented resolution and accuracy. The spatial and temporal variations of the recent geomagnetic field are described by regularly updated geomagnetic field models, such as CHAOS [*Olsen et al.*, 2006] and POMME [*Maus et al.*, 2005, 2010]. These models also include the signature of the quiet time magnetospheric magnetic field and its electromagnetic induction in the rotating Earth [*Maus and Lühr*, 2005]. In addition, a series of geomagnetic models are now provided as official Swarm science products [*Olsen et al.*, 2015]. An interesting phenomenon directly related to the geomagnetic field is the Earth's corotation electric field. It is caused by the rotation of the conducting Earth in its own magnetic field. The geomagnetic field models now enable us to accurately specify the induced corotation charge density and the ensuing electric field, both inside and outside of the corotating region.

Sparked by the unipolar inductor experiment of Faraday, the rotating magnet received considerable attention in the nineteenth century because it was not clear whether the magnetic field lines rotated with the magnet or not. The "moving force line theory" was experimentally disproved [*Kennard*, 1912] in favor of Lorentz' suggestion that the magnetic field lines should be treated as stationary with respect to any nonrotating and unaccelerated frame of reference [*Webster*, 1963]. Consequently, a corotating charge does experience an electric force in the corotating magnetic field. Depending on the conductivity of the magnet and its surroundings, this force is balanced by secondary electric fields of induced corotation charges [*Backus*, 1956].

The Earth's corotation electric field is small in comparison with the field of the global electric circuit [*Volland*, 1985] in the lower atmosphere. Its significance is more obvious in the ionosphere, where electric fields are generally much weaker. Charges induced by rotation migrate into the midlatitude region of closed field lines,

forcing the entire plasmasphere to corotate [*Davis*, 1947; *Hones and Bergeson*, 1965]. Comparing ionospheric dynamo, magnetospheric, and corotation electric fields, *Mozer* [1973] finds that the corotation field is strongest at midlatitudes and diminishes toward the poles. This field is small for the Earth but plays a more significant role in other celestial bodies with stronger magnetic fields, such as in pulsars [*Ruderman and Sutherland*, 1975]. A comprehensive review of pulsar electrodynamics for rotating oblique dipole magnetic fields has recently been provided by *Melrose and Yuen* [2016].

Here a corotation electric field model is derived from Swarm satellite magnetic field measurements, assuming a spherical conducting Earth, surrounded by an insulating lower atmosphere, ionospheric *E* region, and corotating plasmasphere. After discussing reference frames, the relevant equations are derived for inertial and rotating coordinates. A subsequent section discusses a numerical verification of the equations and their implementation. Section 6 then provides illustrations of the primary corotation electric field and the secondary field of the corotation charges for different regions of the Earth system. Of particular interest is the corotation of the plasmasphere. Extreme ultraviolet imager observations by *Sandel et al.* [2003] and *Burch et al.* [2004] show that the plasmasphere rotates slower than the Earth. Another interesting region is the lower atmosphere. As an electrical insulator, it cannot react by charge displacement to the weak corotation electric field. A previous study by *Dumin* [2002] derived vertical electric fields of 50 V/m in the lower atmosphere. Here these fields are found to be significantly smaller. Finally, it is interesting to extend the secondary electric field of the corotation charges outward beyond the corotation region into space. The electric field of the corotation charges is predicted to make an outward directed contribution in the polar regions. However, it is not clear whether this outward electric field plays a role in ion outflows [*Yau and André*, 1997], seen, for example, in measurements of the Defense Meteorological Satellite Program [*Coley et al.*, 2006; *Redmon et al.*, 2010]. A role of the corotation electric field in ion outflows was suggested by *Rothwell* [2003], with subsequent dismissal of *Vasyliunas* [2004] and response by *Rothwell* [2004]. While *Rothwell* [2003] suggests the primary corotation electric field as a source for ion outflows, it is insufficient to only consider the local electromagnetic equations. The equations for the primary corotation electric field and the secondary corotation charges have to be solved with appropriate boundary conditions for the entire Earth system. In a further phenomenon involving corotation electric fields, *Lejosne and Roederer* [2016] discuss their possible influence on the creation of zebra-stripe patterns in the magnetospheric plasma distribution. All of the earlier studies have in common that they consider only the local equations for a dipolar magnetic field. Extending the relevant equations to all degrees and orders of the geomagnetic field and imposing global boundary conditions should add clarity and provide a helpful basis for future investigations of corotation electric field effects.

2. Reference Frames and Coordinates

Here the inertial reference frame which does not take part in Earth rotation is referred to by K. Coordinates corotating with the Earth are denoted by K'. The local velocity vector of Earth rotation in the nonrotating frame at the location $\mathbf{r}$ is given by $\mathbf{u} = \boldsymbol{\Omega} \times \mathbf{r}$, where $\boldsymbol{\Omega} = 2\pi/86400s\hat{\mathbf{z}}$ with unit vector $\hat{\mathbf{z}}$ oriented northward along the Earth rotation axis.

A reference frame corotating with the Earth is not an inertial reference frame. However, one can stipulate that the fields given in rotating coordinates refer to local tangentially comoving inertial frames of reference [*Synge*, 1960; *Irvine*, 1964]. Thus, the system K' is one of locally corotating reference frames. The difference between the noninertial corotating reference frame and the definition of K' used here is illustrated in a simple example: Let us say we have an observer at an equatorial location $\mathbf{R}'$ on the Earth surface. In the noninertial corotating frame, an object at the location $-\mathbf{R}'$ on the opposite side of the Earth would be resting in the corotating frame. However, with our definition of K', the object would actually be moving with twice the Earth rotation velocity relative to the observer. This definition of K' avoids the difficulties of noninertial reference frames while allowing the convenient use of a rotating coordinate system to express the local electromagnetic field and its potentials.

3. Electric Potential and Conductivity Distribution

Using potentials in Coulomb gauge, the potential Φ of the electric field is only a function of the charge density distribution ρ. The electric field in the nonrotating frame K is then given by $\mathbf{E} = -\boldsymbol{\nabla}\Phi_\rho - \partial_t\mathbf{A}$, where $\mathbf{A}$ is

the vector potential of the magnetic field $\mathbf{B} = \nabla \times \mathbf{A}$. A free charge q experiences an electromagnetic force $q(\mathbf{E} + \mathbf{u} \times \mathbf{B})$. *Backus* [1956] showed that for any given corotating magnetic field the charges redistribute in such a way that this force vanishes everywhere within the Earth. At the surface of the Earth, charges are restrained by the insulating atmosphere and can only migrate in the horizontal direction. Hence, we can have a nonvanishing radial electric field on the surface.

Generally speaking, the electric field of the volume charge within the Earth must counterbalance the local field $-\partial_t \mathbf{A} + \mathbf{u} \times \mathbf{B}$ everywhere. Therefore, the charge density is the negative divergence of this term. In the regions where the magnetic field is known, the charge density is therefore readily available. In addition to the volume charge, there may be surface charges at the Earth surface, on the bottom of the ionosphere, and on the outer boundary of the corotation region. The induced charge distribution fulfills boundary conditions at the outer and inner surfaces of the rotating conductor, where its secondary electric field must counterbalance the horizontal component of the primary corotation electric field $\mathbf{E}'_\omega = -\partial_t \mathbf{A} + \mathbf{u} \times \mathbf{B}$.

In terms of electrical conductivity, the Earth and atmosphere can be divided into the following regions:

1. The first region are solid Earth and oceans, all of which are good electrical conductors.
2. The second is the lower atmosphere, which is an insulator up to the bottom of the ionosphere, at about 80 km altitude.
3. The third is ionospheric *E* region up to about 130 km altitude, which is assumed here to be an electrical conductor. The key is that the corotating neutral atmosphere drags along the ions. Above 130 km, the atmosphere becomes so thin and collisions become so rare that the ions are no longer forced into corotation by friction with the neutral atmosphere.
4. The fourth is plasmasphere, which is forced into corotation by the electric potential extending out into space along the region of closed magnetic field lines. This region is assumed to reach 5 Earth radii at the equator, also called "$L = 5$" when using the McIlwain L shell parameter [*McIlwain*, 1961].
5. The last region is the remaining space outside of the *E* region at high latitudes and outside of the corotating plasmasphere at midlatitudes.

It is assumed here that the *E* region behaves like a normal electrical conductor, in the sense that charges are moved by electric fields until the secondary electric field of the induced charges balances the primary corotation electric field. This is realistic for a steady state, but to understand dynamic effects, the strongly anisotropic conductivity of the ionosphere would have to be taken into account.

Outside of the corotation region, magnetospheric convection imposes electric potentials onto the polar ionosphere. Those convection potentials have to be accounted for in a magnetospheric electric field model but are beyond the scope of this work.

4. Derivation of the Electric Potential

The electric field external to the Earth's core, in the nonrotating frame *K* as well as in the system *K*′ of locally corotating reference frames, can be derived for the simplified conductivity structure described above by the following scheme:

1. The electric field $\mathbf{E}$ in *K* is partly due to the rotational change in the magnetic field $\mathbf{E}_\mathbf{A} = -\partial_t \mathbf{A}$ and partly due to an initially unknown induced charge ρ, contributing $\mathbf{E}_\rho = -\nabla \Phi_\rho$.
2. Transforming to corotating coordinates, we can write the electric field in *K*′ as $\mathbf{E}' = \mathbf{E}_\rho + \mathbf{E}_\mathbf{A} + \mathbf{u} \times \mathbf{B} = \mathbf{E}_\rho + \mathbf{E}'_\omega$, where $\mathbf{E}'_\omega = \mathbf{E}_\mathbf{A} + \mathbf{u} \times \mathbf{B}$.
3. For $\mathbf{E}'_\omega = -\nabla \Phi'_\omega$, we can derive the spherical harmonic coefficients of the potential of the primary corotation electric field from the Gauss coefficients of the geomagnetic field. This potential also determines the local volume charge in the region of known magnetic field as $\rho = \epsilon_0 \nabla^2 \Phi'_\omega$. This equation is valid everywhere in the corotating conducting regions.
4. The electric field of the induced charges balances the primary corotation electric field $\mathbf{E}'_\omega$ everywhere inside the corotating conducting regions. On the inner and outer surfaces of the conductor only the tangential fields must cancel, giving $(\mathbf{E}_\rho)_t = -(\mathbf{E}'_\omega)_t$. This determines the charge distribution ρ and its Coulomb potential Φ_ρ.
5. With $\Phi' = \Phi_\rho + \Phi'_\omega + C$ we obtain the spherical harmonic coefficients of Φ' which specify Φ' up to a constant *C*.

6. From the spherical harmonic coefficients of Φ' we can derive equations for the electric field $\mathbf{E}'$ in the system K' of locally corotating reference frames. In any conducting corotating regions $\mathbf{E}' = 0$.
7. Transforming from K' back to K using $\mathbf{E} = \mathbf{E}' - \mathbf{u}\times\mathbf{B}$, we obtain expressions for the electric field in the center fixed inertial frame.

4.1. Step 1: Ansatz for E in *K*

The electric field in K, as seen from an observer not taking part in Earth rotation, is given by

$$\mathbf{E} = \mathbf{E}_\rho + \mathbf{E}_\mathbf{A} = \mathbf{E}_\rho - \partial_t \mathbf{A} \tag{1}$$

$$= \mathbf{E}_\rho - \underbrace{\partial_t' \mathbf{A}}_{=0} + (\mathbf{u}\cdot\nabla)\mathbf{A} - \Omega\times\mathbf{A} \tag{2}$$

$$= \mathbf{E}_\rho + (\mathbf{u}\cdot\nabla)\mathbf{A} - \Omega\times\mathbf{A} \tag{3}$$

where a primed quantity refers to the corotating coordinate system K'. In particular, $\partial_t'\mathbf{A}$ is zero for a corotating magnetic field. For step from (1) to (2) see also *Backus* [1956].

4.2. Step 2: Transform for E From *K* to *K'*

Transforming into K', we can assume $\mathbf{A}' = \mathbf{A}$ because the speed of Earth rotation is slow compared with the speed of light, and the electric field $\mathbf{E}'$ is then given by

$$\mathbf{E}' = \mathbf{E}_\rho + \mathbf{E}_\mathbf{A} + \mathbf{u}\times\mathbf{B} \tag{4}$$

$$= \mathbf{E}_\rho + \mathbf{E}_\omega' \tag{5}$$

where

$$\mathbf{E}_\omega' = \mathbf{E}_\mathbf{A} + \mathbf{u}\times\mathbf{B} \tag{6}$$

$$= \mathbf{E}_\mathbf{A} + \mathbf{u}\times(\nabla\times\mathbf{A}) \tag{7}$$

$$= (\mathbf{u}\cdot\nabla)\mathbf{A} - \Omega\times\mathbf{A} + \mathbf{u}\times(\nabla\times\mathbf{A}) \tag{8}$$

$$= \nabla(\mathbf{u}\cdot\mathbf{A}) \tag{9}$$

$$= -\nabla\Phi_\omega' \tag{10}$$

where $\Phi_\omega' = -\mathbf{u}\cdot\mathbf{A}$. The equivalence of (8) and (9) is shown in Appendix B.

4.3. Step 3: Spherical Harmonic Expansion of Φ_ω' and Induced Charge ρ

The potential Φ_ω' can be derived from the spherical harmonic coefficients of the geomagnetic field as follows:

$$\Phi_\omega' = -\mathbf{u}\cdot\mathbf{A} \tag{11}$$

$$\mathbf{u} = \Omega r \sin\vartheta\hat{\boldsymbol{\varphi}} \tag{12}$$

with $\Omega = |\boldsymbol{\Omega}|$, longitude φ, and colatitude ϑ. Neglecting local currents, the magnetic field is poloidal and can be represented as follows:

$$\mathbf{B} = \nabla\times\mathbf{A} = \nabla\times\Lambda p, \tag{13}$$

where $\Lambda = \hat{\boldsymbol{\varphi}}\partial_\vartheta - (\hat{\boldsymbol{\vartheta}}/\sin\vartheta)\partial_\varphi$ is the surface curl and p is the scalar of the poloidal field [*Backus*, 1986; *Backus et al.*, 1996]. This scalar is related to the usual Gauss coefficients g_ℓ^m of the internal geomagnetic field (with a missing minus sign in *Backus* [1986, equation (58d)] and *Backus et al.* [1996, equation (5.3.15)]) as

$$p(\mathbf{r}) = -\sum_{\ell=1}^{\infty}\sum_{m=-\ell}^{\ell}\frac{a}{\ell}\left(\frac{a}{r}\right)^{\ell+1} g_\ell^m Y_\ell^m(\vartheta,\varphi), \tag{14}$$

where a is the geomagnetic reference radius (6371.2 km) and Y_ℓ^m are the Schmidt seminormalized surface spherical harmonics generally used in geomagnetism (see Appendix A). With

$$\hat{\boldsymbol{\varphi}} \cdot \boldsymbol{\Lambda} = \partial_\vartheta \tag{15}$$

the potential Φ'_ω in equation (11) is

$$\Phi'_\omega(\mathbf{r}) = -\mathbf{u} \cdot \mathbf{A} = -\mathbf{u} \cdot \boldsymbol{\Lambda} p \tag{16}$$

$$= \sum_{\ell=1}^{\infty} \sum_{m=-\ell}^{\ell} \frac{\Omega r a}{\ell} \left(\frac{a}{r}\right)^{\ell+1} g_\ell^m \sin\vartheta \partial_\vartheta Y_\ell^m(\vartheta, \varphi). \tag{17}$$

To write this relation as a spherical harmonic expansion, the term $\sin\vartheta\partial_\vartheta Y_\ell^m$ has to be expressed in spherical harmonics. Then the relation can be rewritten (Appendix C) as

$$\Phi'_\omega(\mathbf{r}) = \sum_{\ell=0}^{\infty} \sum_{m=-\ell}^{\ell} (\Phi'_\omega)_\ell^m(r) Y_\ell^m(\vartheta, \varphi), \tag{18}$$

where

$$(\Phi'_\omega)_\ell^m(r) = \Omega \left(\frac{a}{r}\right)^{\ell+1} f_\ell^m(r), \tag{19}$$

$$\begin{aligned} f_\ell^m(r) = {} & r^2 \frac{\sqrt{(\ell+m)(\ell-m)}}{2\ell-1} g_{\ell-1}^m \\ & - a^2 \frac{(\ell+2)\sqrt{(\ell+m+1)(\ell-m+1)}}{(\ell+1)(2\ell+3)} g_{\ell+1}^m. \end{aligned} \tag{20}$$

Here all coefficients g_ℓ^m with $\ell = 0$ or $\ell < m$ are zero and r is the radius at which Φ'_ω is expanded into spherical harmonics. Thus, the coefficients $(\Phi'_\omega)_\ell^m(r)$ directly follow from the Gauss coefficients g_ℓ^m of the internal geomagnetic field.

For example, the axial magnetic dipole coefficient g_1^0 appears twice in (20) and is responsible for a contribution to the potential ${}_{1,0}\Phi'_\omega$ of

$${}_{1,0}\Phi'_\omega(\mathbf{r}) = -\frac{2a^3\Omega}{3r} g_1^0 Y_0^0 + \frac{2a^3\Omega}{3r} g_1^0 Y_2^0 \tag{21}$$

$$= -\frac{2a^3\Omega}{3r} g_1^0 + \frac{2a^3\Omega}{3r} g_1^0 \frac{1}{2}(3\cos^2\vartheta - 1) \tag{22}$$

$$= \frac{a^3\Omega}{r} g_1^0 (\cos^2\vartheta - 1). \tag{23}$$

Filling in $\Omega = 2\pi/86400$ s, $a = 6371.2$ km, $r = a$, and $g_1^0 = -3 \cdot 10^{-5}$ Vs/m^2 gives a potential at the Earth surface caused by the axial magnetic dipole coefficient g_1^0 of

$${}_{1,0}\Phi'_\omega(\vartheta) = 88\ kV(1 - \cos^2\vartheta), \tag{24}$$

where ϑ is colatitude. At the equator, a potential of 88 kV is comparable with literature values, such as the 92 kV given by *Baumjohann and Treumann* [1997].

4.3.1. Induced Volume Charge ρ

Since the electric field $\mathbf{E}'$ must vanish within the rotating medium,

$$\Phi_\rho = -\Phi'_\omega = \mathbf{u} \cdot \mathbf{A}, \tag{25}$$

a formula originally given by *Backus* [1956]. Thus, the local charge density can be derived by

$$\rho = -\epsilon_0 \nabla^2 \Phi_\rho = \epsilon_0 \nabla^2 \Phi'_\omega. \tag{26}$$

In the magnetic pulsar literature, this is called the Goldreich-Julian charge density, which was derived for a general magnetic field by *Melrose* [1967] as

$$\rho = \epsilon_0(-2\boldsymbol{\Omega} \cdot \mathbf{B} + (\boldsymbol{\Omega} \times \mathbf{r}) \cdot (\boldsymbol{\nabla} \times \mathbf{B})). \tag{27}$$

To express the charge density in spherical harmonics, one can write the Laplacian

$$\nabla^2 = \frac{1}{r^2}\left(\partial_r r^2 \partial_r + \nabla_s^2\right) \tag{28}$$

in terms of the surface gradient [*Backus et al.*, 1996]

$$\boldsymbol{\nabla}_s = r\boldsymbol{\nabla} - \mathbf{r}\partial_r = \hat{\boldsymbol{\vartheta}}\partial_\vartheta + (\hat{\boldsymbol{\varphi}}/\sin\vartheta)\partial_\varphi, \tag{29}$$

and further using

$$\nabla_s^2 Y_\ell^m = -\ell(\ell+1)Y_\ell^m \tag{30}$$

the local volume charge becomes

$$\rho(\mathbf{r}) = -2\epsilon_0\Omega \sum_{\ell=2}^{\infty} \sum_{m=-\ell+1}^{\ell-1} \sqrt{(\ell+m)(\ell-m)} \left(\frac{a}{r}\right)^{\ell+1} g_{\ell-1}^m Y_\ell^m(\vartheta,\varphi). \tag{31}$$

Intermediate steps for the derivation of equation (31) are given in Appendix D.

4.4. Step 4: Coulomb Potential Φ_ρ in the Atmospheric Gap

In the atmospheric gap between the Earth surface, assumed at radius R_- and the bottom of the conducting ionosphere, assumed at radius R_+, we can write the Coulomb potential $\Phi_\rho(\mathbf{r})$ as the sum of an internal potential $\Phi_-(\mathbf{r})$ caused by induced charges interior to the Earth and an external potential $\Phi_+(\mathbf{r})$ caused by induced charges in the ionosphere and corotating plasmasphere. Then the Coulomb potential $\Phi_\rho(\mathbf{r})$ can be expressed as a spherical harmonic expansion:

$$\Phi_\rho(\mathbf{r}) = -\sum_{\ell=0}^{\infty} \sum_{m=-\ell}^{\ell} \left[\left(\frac{R_-}{r}\right)^{\ell+1} (\Phi_-)_\ell^m + \left(\frac{r}{R_+}\right)^{\ell} (\Phi_+)_\ell^m\right] Y_\ell^m(\vartheta,\varphi). \tag{32}$$

The spherical harmonic coefficients $(\Phi_-)_\ell^m$ and $(\Phi_+)_\ell^m$ can be determined from the boundary conditions at R_- and R_+, where the horizontal electric field due to the induced charges has to balance the horizontal part of the primary corotation electric field $\mathbf{E}'_\omega$, as in

$$[\mathbf{E}_\rho(R\hat{\mathbf{r}})]_h = -[\mathbf{E}'_\omega(R\hat{\mathbf{r}})]_h. \tag{33}$$

Since the horizontal electric field on S(R) is completely determined by its potential on that surface, it follows that

$$\Phi_\rho(R\hat{\mathbf{r}}) = -\Phi'_\omega(R\hat{\mathbf{r}}). \tag{34}$$

This leads to two sets of equations with two sets of unknowns $(\Phi_-)_\ell^m$ and $(\Phi_+)_\ell^m$:

$$\left(\frac{R_-}{R_-}\right)^{\ell+1} (\Phi_-)_\ell^m + \left(\frac{R_-}{R_+}\right)^{\ell} (\Phi_+)_\ell^m = -(\Phi'_\omega)_\ell^m(R_-) \tag{35}$$

$$\left(\frac{R_-}{R_+}\right)^{\ell+1} (\Phi_-)_\ell^m + \left(\frac{R_+}{R_+}\right)^{\ell} (\Phi_+)_\ell^m = -(\Phi'_\omega)_\ell^m(R_+). \tag{36}$$

Considering the corotation potential given in equation (19), the spherical harmonic expansion of the Coulomb potential in the atmospheric gap can then be written as follows:

$$\Phi_\rho(\mathbf{r}) = \sum_{\ell=0}^{\infty} \sum_{m=-\ell}^{\ell} (\Phi_\rho)_\ell^m(\mathbf{r}) Y_\ell^m(\vartheta,\varphi) \tag{37}$$

$$\begin{aligned}(\Phi_\rho)_\ell^m(\mathbf{r}) = \frac{-\Omega}{1-\left(\frac{R_-}{R_+}\right)^{2\ell+1}} \Bigg[&\left(\left(\frac{a}{r}\right)^{\ell+1} - \frac{r^\ell a^{\ell+1}}{R_+^{2\ell+1}}\right) f_\ell^m(R_-) \\ &+ \left(\frac{r^\ell a^{\ell+1}}{R_+^{2\ell+1}} - \frac{a^{\ell+1}R_-^{2\ell+1}}{r^{\ell+1}R_+^{2\ell+1}}\right) f_\ell^m(R_+)\Bigg],\end{aligned} \tag{38}$$

where the coefficients $f_\ell^m(r)$ are given by equation (20).

4.5. Step 5: Spherical Harmonic Expansion of Φ'

To derive the electric field in the locally comoving frame, we first derive the scalar potential Φ'. The potential Φ' in K' is the sum of the corotation potential Φ'_ω and the Coulomb potential Φ_ρ, giving

$$\Phi'(\mathbf{r}) = \Phi'_\omega(\mathbf{r}) + \Phi_\rho(\mathbf{r}) \tag{39}$$

$$= \begin{cases} \text{constant} & \text{inside the Earth} \\ \Phi_{\rho \text{of equation (37)}}(\mathbf{r}) + \Phi'_\omega(\mathbf{r}) & \text{atmospheric gap} \\ \text{constant} & \text{inside the ionosphere} \\ \text{constant} & \text{inside the plasmasphere} \\ \Phi_\rho(\mathbf{r}) + \Phi'_\omega(\mathbf{r}) & \text{outside of corotation region.} \end{cases} \tag{40}$$

4.5.1. Atmospheric Gap

Here $\Phi'(\mathbf{r})$ in the atmospheric gap is given by combining (18) and (37) to

$$\Phi'(\mathbf{r}) = \sum_{\ell=0}^{\infty} \sum_{m=-\ell}^{\ell} \left[(\Phi_\rho)^m_\ell(\mathbf{r}) + (\Phi'_\omega)^m_\ell(\mathbf{r})\right] Y^m_\ell(\vartheta, \varphi). \tag{41}$$

4.5.2. Potential Φ' Outside of Corotation Region

The potential in corotating coordinates for $\Phi'(\mathbf{r})$ outside of the corotating region does not have an obvious analytical solution. To approximate it numerically, one has to specify the potential on the outer boundary $\mathbf{r}_{\text{OB}}$ of the corotation region as

$$\Phi_\rho(\mathbf{r}_{\text{OB}}) = -\Phi'_\omega(\mathbf{r}_{\text{OB}}) + C. \tag{42}$$

To find the potential outside of the corotation region, one then has to solve Laplace's equation

$$\nabla^2 \Phi_\rho(\mathbf{r}) = 0 \tag{43}$$

using a numerical method. Here a virtual surface charge density with zero net charge was determined on the boundary. Assuming that the potential decays to zero at infinity, this determines the constant, which was found to be $C \approx 16.3$ kV for a corotation boundary at $L = 5$. Subsequently, for the potential in a locally corotating reference frame, one has to add the corotation potential $\Phi'_\omega(\mathbf{r})$, giving

$$\Phi'(\mathbf{r}) = \Phi_\rho(\mathbf{r}) + \Phi'_\omega(\mathbf{r}). \tag{44}$$

4.6. Step 6: Electric Field E′ in Corotating Coordinate System

The electric field vanishes in the locally corotating frames throughout the conducting regions that corotate with the Earth.

4.6.1. Atmospheric Gap: Horizontal Electric Field $(E')_h$

From equation (34) we see that the potential Φ' is constant at $r = R_-$ and $r = R_+$, which means that the horizontal component of $\mathbf{E}'$ vanishes on the outside and inside surfaces of the conducting regions, as demanded.

For the atmospheric gap ($R_- < r < R_+$), on the other hand, we have

$$(\mathbf{E}')_h = -\frac{1}{r} \boldsymbol{\nabla}_\mathbf{s} \Phi' \tag{45}$$

with the surface gradient

$$\boldsymbol{\nabla}_\mathbf{s} = r\boldsymbol{\nabla} - \mathbf{r}\partial_r = \hat{\boldsymbol{\vartheta}}\partial_\vartheta + (\hat{\boldsymbol{\varphi}}/\sin\vartheta)\partial_\varphi \tag{46}$$

the horizontal components are

$$E'_\varphi(\mathbf{r}) = -\frac{1}{r} \sum_{\ell=0}^{\infty} \sum_{m=-\ell}^{\ell} \left[(\Phi_\rho)^m_\ell(\mathbf{r}) + (\Phi'_\omega)^m_\ell(\mathbf{r})\right] \frac{\partial_\varphi}{\sin\vartheta} Y^m_\ell(\vartheta, \varphi) \tag{47}$$

$$E'_\vartheta(\mathbf{r}) = -\frac{1}{r} \sum_{\ell=0}^{\infty} \sum_{m=-\ell}^{\ell} \left[(\Phi_\rho)^m_\ell(\mathbf{r}) + (\Phi'_\omega)^m_\ell(\mathbf{r})\right] \partial_\vartheta Y^m_\ell(\vartheta, \varphi). \tag{48}$$

4.6.2. Atmospheric Gap: Radial Electric Field E'_r

From the radial derivative of the potential Φ' we obtain the radial electric field

$$\begin{aligned} E'_r(\mathbf{r}) &= -\partial_r \Phi' \\ &= -\sum_{\ell=0}^{\infty} \sum_{m=-\ell}^{\ell} [\partial_r (\Phi_\rho)^m_\ell(\mathbf{r}) + \partial_r (\Phi'_\omega)^m_\ell(\mathbf{r})] Y^m_\ell(\vartheta, \varphi), \end{aligned} \tag{49}$$

where

$$\begin{aligned} \partial_r (\Phi_\rho)^m_\ell(\mathbf{r}) = \frac{\Omega}{1 - \left(\frac{R_-}{R_+}\right)^{2\ell+1}} \Bigg[&\frac{\ell+1}{a} \left(\frac{a}{r}\right)^{\ell+2} + \frac{\ell r^{\ell-1} a^{\ell+1}}{R_+^{2\ell+1}} f^m_\ell(R_-) \\ &- \left(\frac{\ell r^{\ell-1} a^{\ell+1}}{R_+^{2\ell+1}} + \frac{(\ell+1) a^{\ell+1} R_-^{2\ell+1}}{r^{\ell+2} R_+^{2\ell+1}} \right) f^m_\ell(R_+) \Bigg] \end{aligned} \tag{50}$$

$$\begin{aligned} \partial_r (\Phi'_\omega)^m_\ell(\mathbf{r}) &= \frac{-(\ell+1)\Omega}{a} \left(\frac{a}{r}\right)^{\ell+2} f^m_\ell(r) + \Omega \left(\frac{a}{r}\right)^{\ell+1} \partial_r f^m_\ell(r), \\ \partial_r f^m_\ell(r) &= 2r \frac{\sqrt{(\ell+m)(\ell-m)}}{2\ell-1} g^m_{\ell-1}. \end{aligned} \tag{51}$$

In contrast to the horizontal component, the radial electric field does not vanish on the surface of the Earth and the inner boundary of the ionosphere.

4.6.3. Outside of Corotating Region

The electric field outside of the corotating region has to be numerically computed similar to the potential $\Phi_\rho(\mathbf{r})$, found by solving equation (43) and adding the corotation electric field $\mathbf{E}'_\omega$ as

$$\mathbf{E}'(\mathbf{r}) = -\nabla \Phi_\rho(\mathbf{r}) - \nabla \Phi'_\omega(\mathbf{r}). \tag{52}$$

4.7. Step 7: Electric Field E in the Inertial Frame

One could derive the electric field in the inertial frame from the potentials $\mathbf{E} = -\nabla \Phi_\rho - \partial_t \mathbf{A}$. However, it may be easier to just transform the electric field $\mathbf{E}'$ from K' back to K as

$$\mathbf{E} = \mathbf{E}' - \mathbf{u} \times \mathbf{B} \tag{53}$$

$$= \mathbf{E}' - u\hat{\boldsymbol{\varphi}} \times (B_r \hat{\mathbf{r}} + B_\vartheta \hat{\boldsymbol{\vartheta}} + B_\varphi \hat{\boldsymbol{\varphi}}) \tag{54}$$

$$= \mathbf{E}' - uB_r \hat{\boldsymbol{\vartheta}} + uB_\vartheta \hat{\mathbf{r}}. \tag{55}$$

4.7.1. Horizontal Electric Field $(E)_h$

The first thing to notice from equation (55) is that the φ component of the electric field is the same in K and K', which is the consequence of a velocity $\mathbf{u}$ in the φ direction. Hence,

$$E_\varphi = E'_\varphi. \tag{56}$$

For E'_ϑ, on the other hand, we have to subtract uB_r, giving

$$E_\vartheta(\mathbf{r}) = E'_\vartheta(\mathbf{r}) - \Omega r \sum_{\ell=1}^{\infty} \sum_{m=-\ell}^{\ell} (\ell+1) \left(\frac{a}{r}\right)^{\ell+2} g^m_\ell \sin\vartheta Y^m_\ell(\vartheta, \varphi). \tag{57}$$

Hence, in the inertial frame K we generally have a nonzero horizontal electric field at the surface of the conductor, as illustrated in section 6 below.

4.7.2. Radial Electric Field E_r

Starting from equation (55), we have

$$\mathbf{E} = \mathbf{E}' - uB_r \hat{\boldsymbol{\vartheta}} + uB_\vartheta \hat{\mathbf{r}} \tag{58}$$

$$= \mathbf{E}_\rho + \mathbf{E}'_\omega - uB_r \hat{\boldsymbol{\vartheta}} + uB_\vartheta \hat{\mathbf{r}}. \tag{59}$$

Remembering from (9) that $\mathbf{E}'_\omega = \nabla(\mathbf{u}\cdot\mathbf{A})$ and substituting $B_\vartheta = (\nabla\times\mathbf{A})\cdot\hat{\vartheta}$, we get

$$E_r = (\mathbf{E}_\rho)_r + \partial_r(\mathbf{u}\cdot\mathbf{A}) - u[(\nabla\times\mathbf{A})\cdot\hat{\vartheta}] \tag{60}$$

$$= (\mathbf{E}_\rho)_r + \partial_r(\mathbf{u}\cdot\mathbf{A}) + \frac{u}{r\sin\vartheta}[\partial_\varphi A_r - \sin\vartheta\partial_r rA_\varphi] \tag{61}$$

$$= (\mathbf{E}_\rho)_r + \partial_r(uA_\varphi) + \Omega\partial_\varphi A_r - \partial_r\Omega r\sin\vartheta A_\varphi \tag{62}$$

$$= (\mathbf{E}_\rho)_r + \Omega\partial_\varphi \underbrace{A_r}_{=0} \tag{63}$$

$$= (\mathbf{E}_\rho)_r, \tag{64}$$

where always $A_r = 0$ for a poloidal geomagnetic field because $\mathbf{A} = \Lambda p$. Hence, in the center fixed inertial frame the radial component of the electric field is equal to the electrostatic field of the induced corotation charges. Outside of the corotation region, this radial component of the electrostatic field has to be found numerically. The interesting consequence is that the radial electric field is significantly different from zero at the poles, even though $\mathbf{u}\times\mathbf{B}$ vanishes here, as illustrated in the figures below.

5. Numerical Validations

Here two validations are proposed. One is for the primary corotation electric field and the other for the virtual surface charge on the outer boundary.

5.1. Validation of Corotation Electric Field

The correct implementation of the equations can be verified numerically. Equation (18) in Step 3 gives the spherical harmonic expansion of Φ'_ω. Its gradient gives the corotation electric field in the corotating frame, $\mathbf{E}'_\omega = -\partial_t\mathbf{A} + \mathbf{u}\times\mathbf{B}$. This relation can be numerically verified by comparing the left side computed from the gradient of (18) with right side computed as follows: The vector potential of the magnetic field $\mathbf{A}$ is related to the poloidal scalar p according to equation (13) as $\mathbf{A} = \Lambda p$. From the spherical harmonic expansion of p, given by equation (14), one can determine the expansion of the components of $\mathbf{A}$ as follows:

$$A_r = 0 \tag{65}$$

$$A_\vartheta = a\sum_{\ell=1}^{\infty}\sum_{m=-\ell}^{\ell}\frac{1}{\ell}\left(\frac{a}{r}\right)^{\ell+1} g_\ell^m \frac{\partial_\varphi Y_\ell^m(\vartheta,\varphi)}{\sin\vartheta} \tag{66}$$

$$A_\varphi = -a\sum_{\ell=1}^{\infty}\sum_{m=-\ell}^{\ell}\frac{1}{\ell}\left(\frac{a}{r}\right)^{\ell+1} g_\ell^m \partial_\vartheta Y_\ell^m(\vartheta,\varphi). \tag{67}$$

To validate the corotation electric field $\mathbf{E}'_\omega(r,\vartheta,\varphi)$, one can then compute the vector potential $\mathbf{A}$ at the locations $(r,\vartheta,\varphi+d\varphi)$ and $(r,\vartheta,\varphi-d\varphi)$, where $d\varphi$ is a small angular offset, and compute the temporal derivative of $\mathbf{A}$ as follows:

$$-\partial_t\mathbf{A} = \frac{\Omega}{2d\varphi}(\mathbf{A}(r,\vartheta,\varphi+d\varphi) - \mathbf{A}(r,\vartheta,\varphi-d\varphi)). \tag{68}$$

Adding $\mathbf{u}\times\mathbf{B}$ then gives $\mathbf{E}'_\omega$, verifying the correctness of the equations and the accuracy of their numerical implementation.

5.2. Validation of Surface Charge on the Outer Boundary

The 3-D charge can be represented by a virtual surface charge on the boundary of the corotation region. This boundary charge density is found numerically by matching its electric potential to the negative of the corotation potential on the boundary. The result of a conjugate-gradient implementation is illustrated for an east-west slice in Figure 1. The method converged without difficulties for a 720×1440 cell latitude-longitude grid on the boundary of the corotation region. The slice in Figure 1 shows the corotation potential on the boundary of the corotation region (red) versus the Coulomb potential of the virtual surface charge. The excellent agreement means that the surface charges succeed in representing the Coulomb potential of the corotation charges on the boundary. The two humps are at the top of the northern and southern polar ionosphere. The lines between the two humps follow the outermost closed field lines at the −85° and 95°

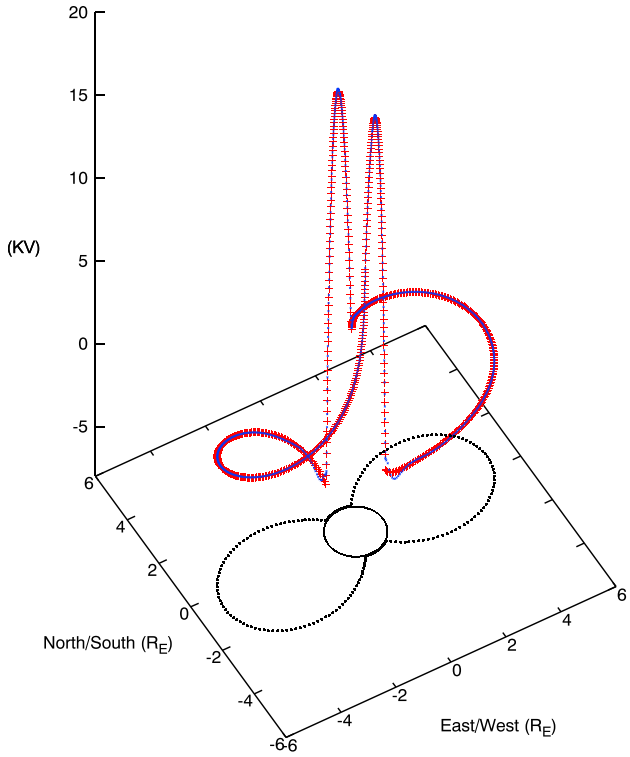

Figure 1. Shown here as a validation example is the negative of the corotation potential (red) against the Coulomb potential of the numerically determined virtual surface charge (blue) on the boundary of the corotation region for a cross section through the plasmasphere at the −85° to 95° geographic meridian. The match is very good, apart from small differences where the boundary of the corotating plasmasphere intersects the high-latitude ionosphere.

geographic meridians, which were arbitrarily chosen for this example. For an axially symmetric field, the potential would be constant along those field lines. It is interesting to see here how much the potential actually changes along the field lines for the real magnetic field, which is not axially symmetric.

6. Results

The equations derived here can now be used to shed some light on several aspects of the Earth system. The following sections discuss the corotation charge density, the balance between corotation electric field and the secondary field of corotation charges, the polar radial electric field, the electric field in the atmospheric gap, and the corotation lag of the plasmasphere.

6.1. Corotation Charge Density

Using the tenth generation of the POMME geomagnetic model derived from Swarm measurements, the induced charge density can be computed from the core-mantle boundary to the plasmapause (Figure 2). The corotation charge density in the Earth's core cannot be computed because the magnetic field is not known there.

6.2. Balance Between Corotation Electric Field and the Secondary Field of Corotation Charges

The corotation charge is caused by the primary corotation electric field (Figure 3), which causes the redistribution of electrical charges within the conducting corotating region. The Coulomb electric field of these corotation charges (Figure 4) cancels out the primary corotation electric field $\mathbf{E}'_\omega$. Figure 5 shows the complete field $\mathbf{E}'_\omega$ versus only the $\mathbf{u} \times \mathbf{B}$ term, illustrating the importance of the contribution from the $\partial_t \mathbf{A}$ term. This term also causes changes of Φ'_ω along field lines through the plasmasphere. The contribution of the $\partial_t \mathbf{A}$ and the $\mathbf{u} \times \mathbf{B}$ terms to the primary corotation electric field $\mathbf{E}'_\omega$ is further illustrated in Figure 6 for a profile of the northward component along the geographic equator at the top of the ionospheric *E* region. Due to the $\partial_t \mathbf{A}$ contribution, $\mathbf{E}'_\omega$ is, in general, not perpendicular to the geomagnetic field lines. An interesting consequence of this is that the corotation potential changes along the geomagnetic field lines.

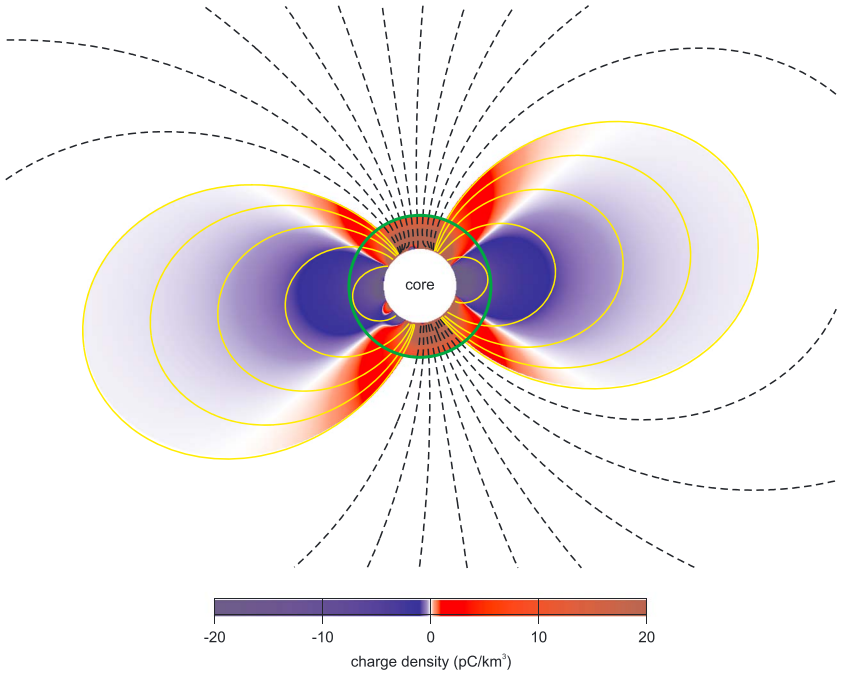

Figure 2. Cross section through the Earth at the −85° to 95° geographic meridian, which was chosen to illustrate the tilt of the geomagnetic dipole. The corotation charge density is displayed from the core-mantle boundary to the plasmapause, according to equation (31) for the present geomagnetic field. The surface of the Earth and the top of the ionospheric *E* region are only 130 km apart and therefore lie within the green line. Closed field lines for $L = 1$ to $L = 5$ are shown in yellow. Outside this region magnetic field lines are shown by dashed lines in black. Units of the charge density are 10^{-12} C/km^3.

6.3. Outside Electric Field in the Corotating Frame

Outside of the corotating region, the corotation charges generate an electric field, which is displayed in Figure 7 in terms of its Coulomb potential. This potential peaks at the poles with about 16 kV and falls off to zero to all sides with increasing distance from the Earth.

Along the Earth rotation axis the radial component of the primary corotation electric field vanishes because the velocity is zero and $A_r = 0$. Correspondingly, the Coulomb electric field is also zero along the spin axis within the corotation region. However, this is no longer true outside of the corotation region. A profile of the Coulomb potential along the Earth rotation axis is shown in Figure 8. The Coulomb potential is constant inside the corotating region and falls off by about 16 kV above the polar ionosphere due to the "missing" positive corotation charges above the poles, which would balance the polar charges within the corotation region.

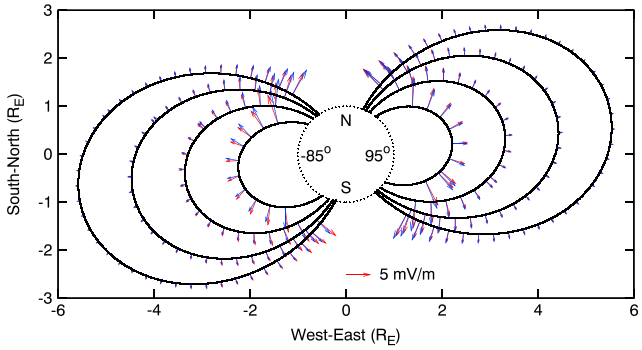

Figure 3. The primary corotation electric field $\mathbf{E}'_\omega$ in the corotating frame K' falls off with increasing distance from the Earth because the geomagnetic field magnitude decreases faster than the tangential velocity increases. Geomagnetic field lines for $L = 2$ to $L = 5$ are displayed in black. The complete corotation electric field is shown in red, while the $\mathbf{u} \times \mathbf{B}$ component is shown in blue.

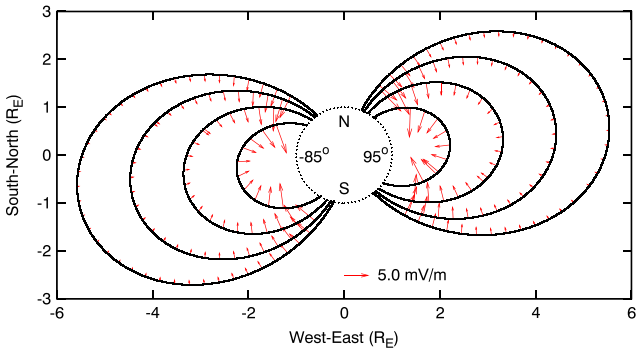

Figure 4. The electric field of the corotation charges $\mathbf{E}_\rho$ (shown in red on the geomagnetic field lines for $L = 2$ to $L = 5$) balances the primary corotation electric field (Figure 3) in the corotating frame K'.

Figure 9 shows a corresponding profile in the locally corotating frame radially outward through the equator at the 95° meridian. Here the corotation electric field is not zero. Its corotation potential balances the Coulomb potential inside of the corotating region. The combined potential in the locally corotating frame is therefore constant within the corotating region and falls off to zero with increasing distance from the Earth.

Staying in the system K' of locally corotating reference frames, Figure 10 shows the primary corotation electric field caused by Earth rotation in its own magnetic field. This corotation electric field is responsible for the positive corotation charge accumulation in the northern and southern polar regions. It also causes the negative corotation charge accumulation at low northern and southern latitudes (see Figure 2). Figure 11 then shows the secondary Coulomb electric field in the northern polar region caused by the combined corotation charges of the entire corotating region. The missing positive corotation charges above the northern ionosphere create a significant outward electric field. The combined electric field in K' is then shown in Figure 12.

6.4. External Electric Field in the Inertial Frame

Outside of the corotating region, it may be advantageous to describe the electric field in an inertial frame that does not take part in Earth rotation. Figure 13 shows the north polar electric field in the inertial reference frame. This field is the sum of the Coulomb electric field and the electric field caused by the changing

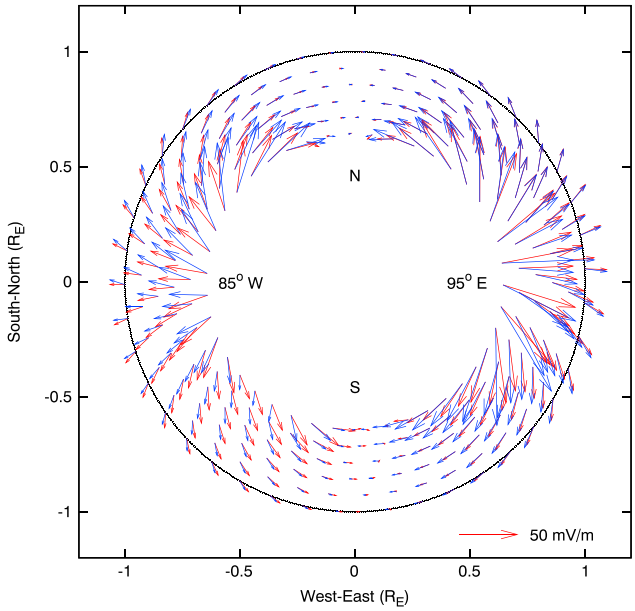

Figure 5. For the corotating frame K', the primary corotation electric field $\mathbf{E}'_\omega$ inside the Earth is shown here in red, while the $\mathbf{u} \times \mathbf{B}$ component is shown in blue. Any residual electric field in the corotating frame would cause a redistribution of charges within the conducting regions of the Earth until the total field cancels to zero. This figure further illustrates that the $\partial_t \mathbf{A}$ component makes a significant contribution to the corotation electric field.

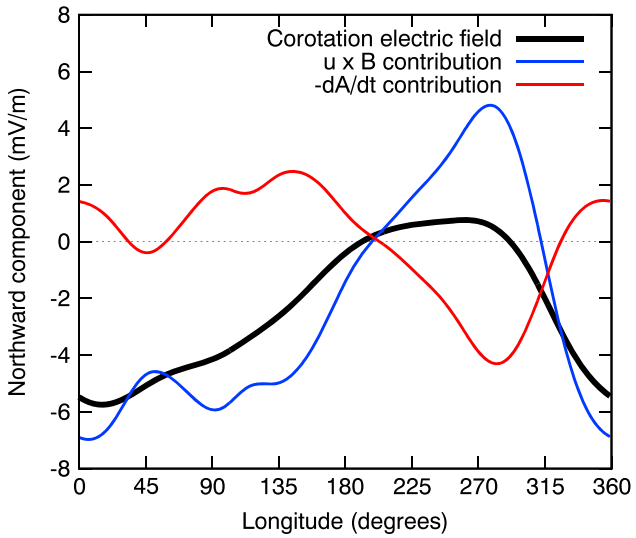

Figure 6. The contribution of $\partial_t \mathbf{A}$ (red) and $\mathbf{u} \times \mathbf{B}$ (blue) to the primary corotation electric field $\mathbf{E}'_{\omega}$ (black) is illustrated here in the corotating frame K' for a profile of the northward component along the geographic equator at the height of the top of the ionospheric E region.

magnetic field $\partial_t \mathbf{A}$. Here it was instead computed by transforming the electric field shown in Figure 12 from the locally corotating frames to the inertial frame. Figure 14 then gives a global view of the electric field in the inertial frame outside of the corotating region. The largest electric field strengths are seen in the northern and southern polar regions where the upper atmosphere does not corotate.

6.5. Electric Field in the Atmospheric Gap

The assumption that the corotation electric field is balanced by corotation charges is only valid if the electrical charges can move freely in the medium. This is the case in the Earth and the ionosphere but not in the lower atmosphere. Assuming that the atmosphere from the surface to 80 km altitude behaves like an electrical insulator without corotation charges, an uncompensated electric field results, as shown in Figure 15, in the system K' of locally corotating reference frames. This field is primarily vertical, pointing upward at the Earth surface in the north and south polar regions and pointing downward in the equatorial region. Of the order

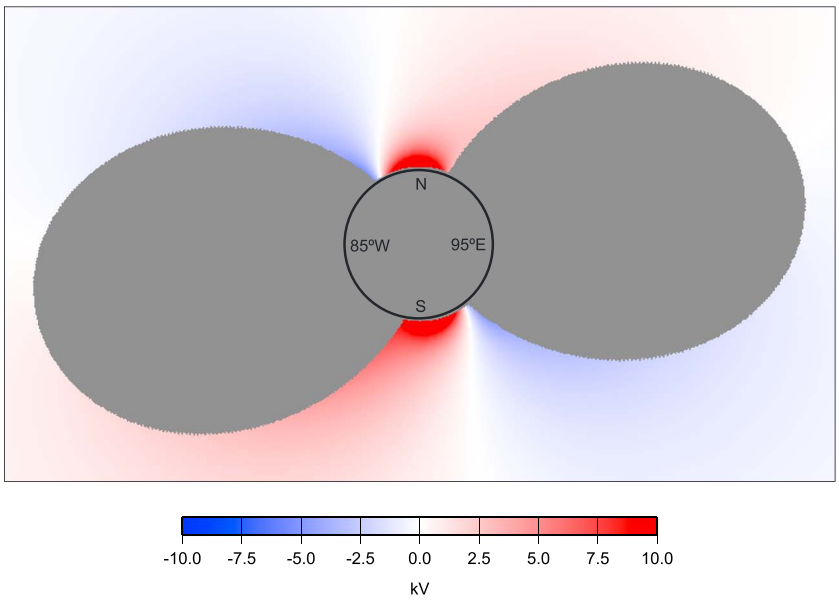

Figure 7. The Coulomb potential outside of the corotating region peaks at the poles with about 16 kV and falls off to zero to all sides with increasing distance from the Earth. This applies to both the corotating and nonrotating frames.

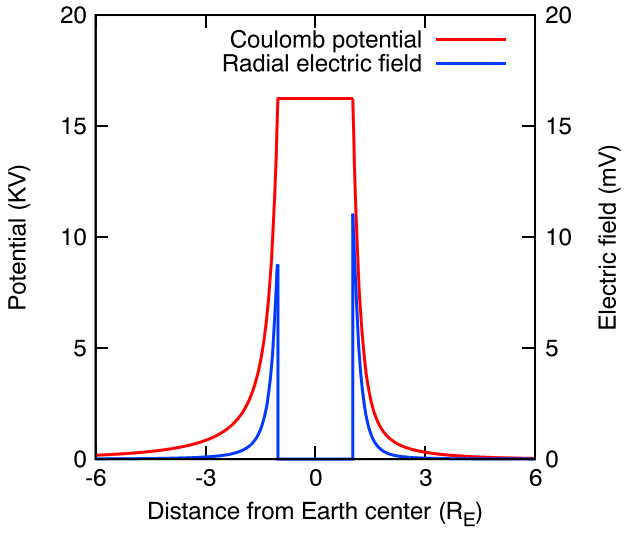

Figure 8. Profile of the Coulomb potential along the Earth rotation axis outward through the geographic North Pole. Negative *x* values correspond to the Southern Hemisphere. The Coulomb potential is constant inside the corotating region and falls off by about 16 kV above the polar ionosphere. This applies to both the corotating and nonrotating frames of reference.

of 0.3 mV/m, this field is very weak compared to other atmospheric electric field sources. In a previous study, *Dumin* [2002] derived relations for the corotation potential similar to equation (24) and considered the effect of a highly resistive atmospheric layer. It was assumed that the top of the atmospheric layer was electrically connected to space, so that the entire potential drop would occur over the atmospheric layer. A vertical electric field of 50 V/m was then inferred as the gradient of the corotation potential. This is 5 orders of magnitude larger than the vertical electric field derived here. Dumin's paper does not specify the values used for the input parameters. Nevertheless, two factors may explain the discrepancy: The first concerns the assumed thickness of the resistive atmosphere. Considering the 88 kV amplitude in equation (24) for the corotation potential and a resistive atmospheric layer of about 80 km, the vertical electric field derived from Dumin's model should be closer to 1 V/m than to 50 V/m. It is therefore likely that Dumin assumed a much thinner resistive atmosphere. Second, Dumin's model omits a conducting ionospheric layer, which is included in the present model. Corotating with the Earth, the ionospheric layer has a corotation potential very similar to the corotation potential

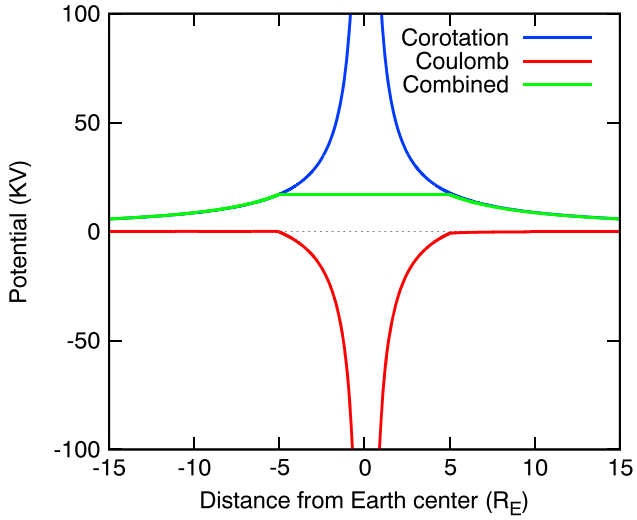

Figure 9. Profile in the locally corotating frame K' through the Earth center in the equatorial plane intersecting the −85° and 95° meridians. The corotation potential (blue) balances the Coulomb potential (red) inside of the corotating region. The total potential in the locally corotating frame (green) is constant within the corotating region and falls off to zero on both sides with increasing distance from the Earth.

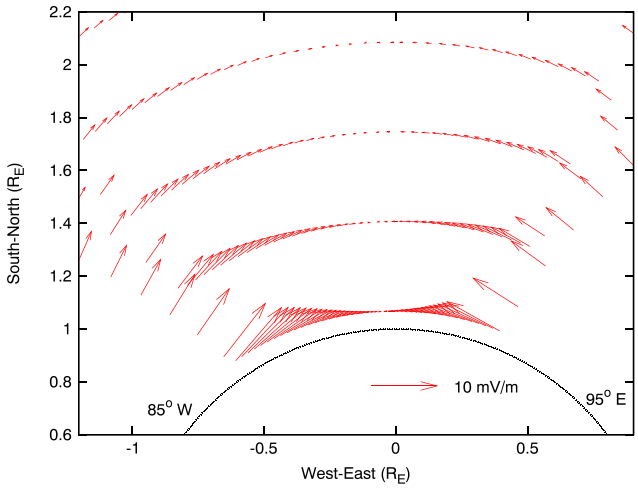

Figure 10. Primary corotation electric field $\mathbf{E}'_{\omega}$ in the north polar region in the locally corotating frame K' caused by Earth rotation in its own magnetic field. This primary electric field is responsible for the secondary effect of a positive corotation charge accumulation in the northern and southern polar regions.

at the Earth surface. Therefore, including such a conducting ionospheric layer further significantly reduces the predicted strength of the vertical corotation electric field in the lower atmosphere, explaining the large difference between the two models.

6.6. Corotation and Underrotation of the Plasmasphere

It is well known that the secondary electric field of the corotation charges forces the plasmasphere into corotation. However, this argument has primarily been made for dipolar magnetic fields. It is worth revisiting this topic for the actual Earth magnetic field. First, let us consider the simpler situation of an axially symmetric magnetic field, which can include higher-degree zonal harmonics. In this case, the term $-\partial_t \mathbf{A}$ vanishes and the corotation electric field reduces to $\mathbf{E}'_{\omega} = \mathbf{u} \times \mathbf{B}$. Consequently, the secondary electric field of the corotation charges becomes $-\nabla\Phi_{\rho} = \mathbf{E}'_{\rho} = -\mathbf{E}'_{\omega} = -\mathbf{u} \times \mathbf{B}$. This equation is valid in the ionospheric E region up to about 130 km altitude. An observer above the E region, who is not taking part in Earth rotation, would not see any changes in the assumed axially symmetric geomagnetic field. Electric charges can move unobstructed along geomagnetic field lines. Furthermore, the gradient of the potential $\nabla\Phi_{\rho} = \mathbf{u} \times \mathbf{B}$ is perpendicular to the geomagnetic field lines. Consequently, electric charges will move out along a closed geomagnetic field line until the entire line is brought to the same potential. As a consequence, the plasmasphere assumes exactly the

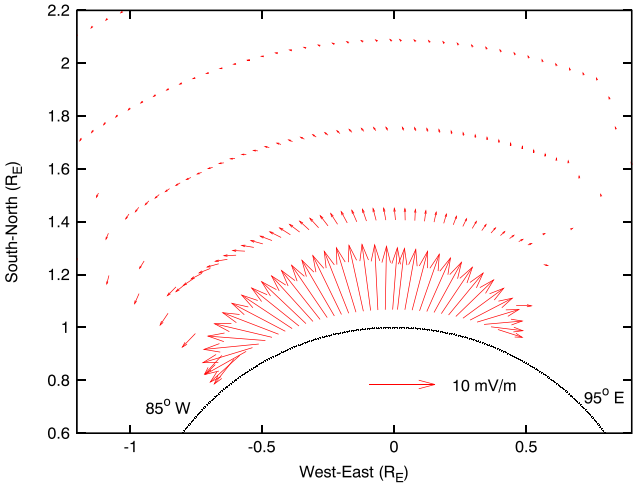

Figure 11. Coulomb electric field in the north polar region caused by the combined corotation charges of the entire corotating region. The missing positive corotation charges above the northern ionosphere create a significant outward electric field. This is applicable in both the corotating and nonrotating reference frames.

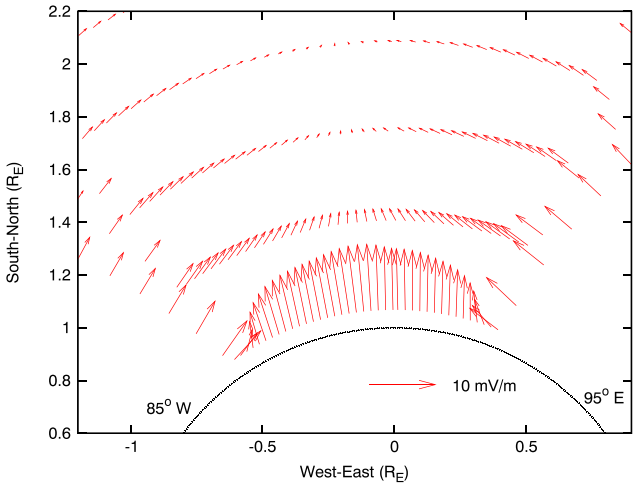

Figure 12. Combined electric field in the system K' of locally corotating reference frames. This field, which is the sum of the contributions shown in Figures 10 and 11, must be perpendicular to the outer boundary of the corotation region.

potential that it would assume if it were part of a corotating conductor. The electric field in the inertial frame then becomes $-\mathbf{u} \times \mathbf{B}$. The plasma drifts with a velocity $\mathbf{u}^{\text{drift}}$ of

$$\mathbf{u}^{\text{drift}} = \frac{\mathbf{E} \times \mathbf{B}}{B^2} \tag{69}$$

$$= \frac{(-\mathbf{u} \times \mathbf{B}) \times \mathbf{B}}{B^2} \tag{70}$$

$$= \mathbf{u} - \frac{\mathbf{B} \cdot \mathbf{u}}{B^2}\mathbf{B} \tag{71}$$

$$= \mathbf{u}, \tag{72}$$

where the second term in (71) vanishes for an axially symmetric magnetic field because $\mathbf{B}$ is then perpendicular to $\mathbf{u}$. This means that the plasma within the region of closed field lines is forced into exact corotation with the Earth.

This line of reasoning can now be extended to the actual geomagnetic field, which is not axisymmetric. In this case, the potential at the top of the E region fulfills

$$-\nabla\Phi_\rho = -\mathbf{E}'_\omega = \partial_t \mathbf{A} - \mathbf{u} \times \mathbf{B}. \tag{73}$$

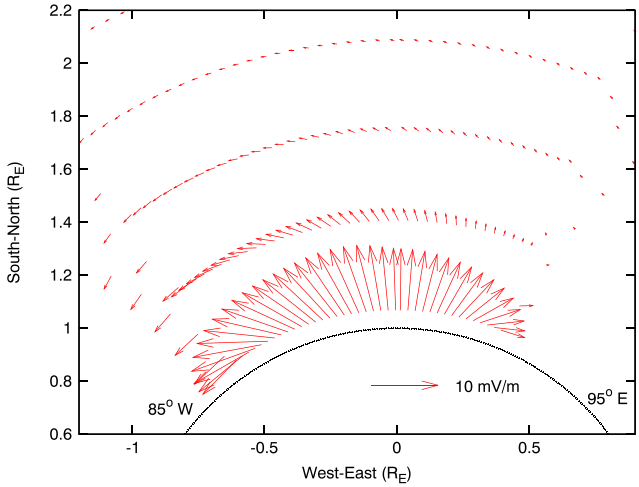

Figure 13. Electric field in the inertial reference frame K, computed here by transforming the electric field shown in Figure (12) from the rotating to the inertial frame for the same meridional cross section. The electric field at the boundary of the corotating region now has a tangential component, which was absent in the corotating frame.

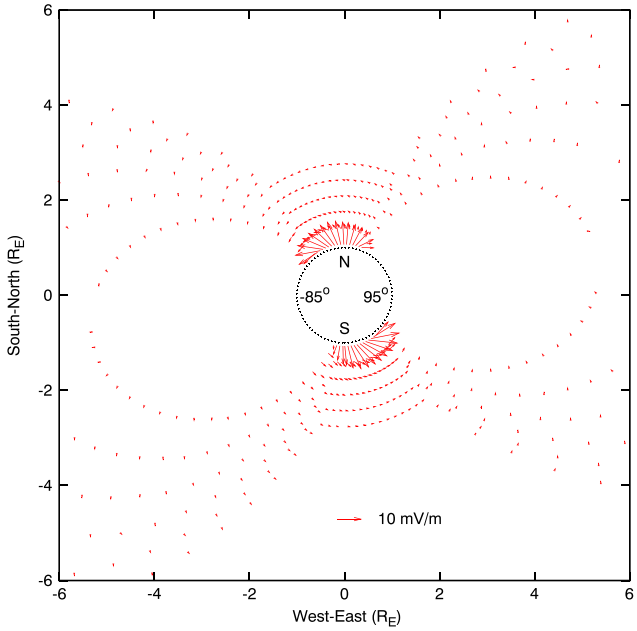

Figure 14. Global view of the electric field in the inertial frame K outside of the corotating region, assumed here to be bounded by $L = 5$. The largest electric fields are predicted for the northern and southern polar regions where the atmosphere does not corotate. In reality, these polar electric fields may be compensated by additional surface and volume charges and are masked by magnetospheric convection.

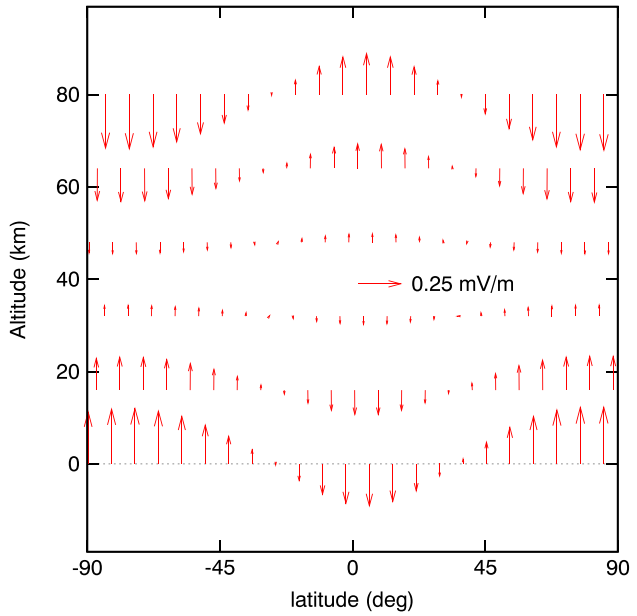

Figure 15. Combined electric field along the 95° meridian in the system K' of locally corotating reference frames in the lower atmosphere. The rectangular area corresponds to a slice through the thin shell from the Earth surface to the bottom of the ionosphere, assumed here at 80 km altitude. The vectors are vertical not because of the distortion of the projection but because they are actually almost entirely aligned with the radial direction. These corotation electric fields are very small compared to the fields of the global electric circuit.

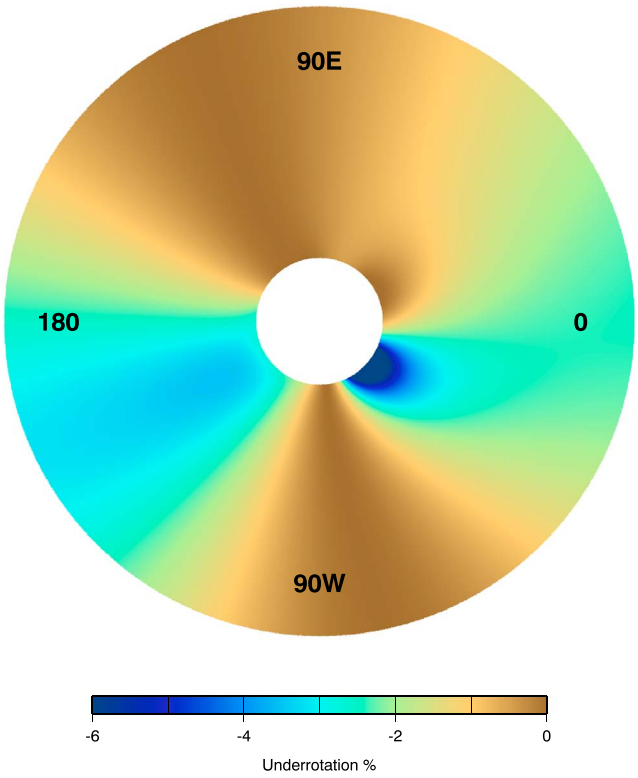

Figure 16. Shown here is an equatorial slice through the plasmasphere out to about $L = 5$, with the longitude sectors indicated in degrees. Colors indicate the magnitude of the corotation lag in percent if the plasma drift were solely caused by the corotation electric field. The strongest underrotation of up to 12% would be predicted for the region of the South Atlantic anomaly, where the geomagnetic field lines exhibit the largest departure from the geographic north direction. However, actual rotation of the plasmasphere is influenced by further effects, such as Fermi acceleration and electric fields due to ionospheric winds.

Thus, the potential is no longer constant along the geomagnetic field lines, as seen, for example, in Figure 1. The potential at a point on a geomagnetic field line exiting the ionospheric E region in the south will, in general, be different from the potential at the point where the field line reenters the ionosphere in the north. This potential difference on its own would cause an electric current to flow along the magnetic field line from one hemisphere to the other. However, in the inertial frame there is now an additional electric field $-\partial_t \mathbf{A}$. This electric field happens to exactly counteract the potential difference along the magnetic field line, as seen in equation (73). Therefore, we again arrive at a stable corotation charge distribution in the plasmasphere. The resulting electric field in the inertial frame is then

$$\mathbf{E} = -\nabla\Phi_\rho + \mathbf{E}_A \tag{74}$$

$$= \partial_t \mathbf{A} - \mathbf{u} \times \mathbf{B} - \partial_t \mathbf{A} \tag{75}$$

$$= -\mathbf{u} \times \mathbf{B}. \tag{76}$$

Referring back to equation (69), the corresponding plasma drift then takes the same form as in equation (70). However, in this case $\mathbf{B}$ is no longer perpendicular to $\mathbf{u}$. Considering the drift velocity only in the longitudinal φ direction, we obtain

$$u_\varphi^{\text{drift}} = \mathbf{u} - \frac{\mathbf{B} \cdot \mathbf{u}}{B^2} B_\varphi \tag{77}$$

$$= \left(1 - \frac{(\mathbf{B} \cdot \mathbf{u})^2}{B^2 u^2}\right) \mathbf{u}. \tag{78}$$

This means that the longitudinal drift velocity u_φ^{drift} is, in general, smaller than the Earth velocity $\mathbf{u}$, as already pointed out for obliquely rotating pulsars by *Melrose and Yuen* [2012]. Depending on the local angle between the geomagnetic field and the φ direction, the plasma would underrotate relative to the Earth. The underrotation percentage is illustrated for an equatorial slice of the plasmasphere in Figure 16. Predicted underrotation percentages would be of the order of a few percent. However,

as discussed by *Hones and Bergeson* [1965], the plasma particles further experience Fermi acceleration when bouncing back and forth along the field lines between the mirror points. Consequently, their kinetic energy as seen in the rest frame is slightly greater when their motion is in the direction of Earth rotation than when it is in the opposite direction. This additional acceleration exactly compensates for the underrotation predicted from the corotation electric field alone. A complete understanding of plasmasphere corotation further has to take electric fields from ionospheric winds into account, which may be responsible for the 10% to 15% observed by *Sandel et al.* [2003] and *Burch et al.* [2004].

7. Discussion

Rotation of the Earth in its own geomagnetic field leads to a redistribution of charge in such a way that the electrostatic field counterbalances the primary corotation electric field $\mathbf{E}'_\omega = -\partial_t \mathbf{A} + \mathbf{u} \times \mathbf{B}$ throughout the conducting Earth and the corotating plasmasphere. This charge density has been derived here for a given spherical harmonic expansion of the geomagnetic potential, derived from measurements of the Swarm satellite constellation. The charge is positive at high latitudes, negative at midlatitudes, and increases strongly toward the Earth's core. The electric field outside of the Earth depends on the boundary conditions applicable at the surface of the corotating region. In the computations here, it was assumed that the net electrostatic corotation charge of the Earth is zero. But depending on the boundary conditions imposed by the magnetosphere, the Earth could actually carry a net electric charge.

The electric field in the corotating conducting regions cancels out to zero in the corotating frame, whereas in the insulating atmosphere and outside of the corotating plasmasphere, the corotation charges create a net electric field. Based on the review of previous studies, three regions were identified here in which accurate specification of corotation electric fields could lead to new insights for the Earth system.

1. In the region of closed magnetic field lines, the plasmasphere was previously known to be forced into corotation. As pointed out by *Melrose and Yuen* [2012] for obliquely rotating pulsars, accounting for the actual geomagnetic field geometry leads to a prediction of underrotation in certain longitudinal sectors. However, a complete understanding of plasma underrotation has to account for all sources of drift, including Fermi acceleration [*Hones and Bergeson*, 1965]. In any case, the predicted underrotation would be smaller than the corotation lag observed by *Sandel et al.* [2003]. This could be caused by a corresponding corotation lag of the neutral atmosphere at *E* region altitudes and should be investigated further.
2. Since the lower atmosphere is nonconducting, corotation charges in the Earth and upper atmosphere are expected to create an uncompensated electric field there. We find that this field is primarily vertical and of the order of 0.3 mV/m, which is significantly smaller than the 50 V/m derived in a previous study by *Dumin* [2002].
3. While it is well known that the primary corotation electric field is canceled locally by the secondary field of corotation charges, the question remains of how these electric fields extend into the surrounding space that does not take part in corotation. Here it is estimated that the corotation charges contribute a potential of about 16 kV to the polar regions, resulting in outward fields of about 10 mV/m. Of course, these corotation electric fields cannot be considered in isolation. They may be compensated by surface and volume charges, and they may be masked by magnetospheric convection electric fields.

Appendix A: Definition of Schmidt Seminormalized Spherical Harmonics

The Schmidt seminormalized spherical harmonic basis functions $Y_\ell^m(\vartheta, \varphi)$ [*Backus et al.*, 1996, pp. 141–142] are defined as

$$Y_\ell^m = \cos m\varphi \, \check{P}_\ell^m(\cos\vartheta), \quad 0 \le m \le \ell \tag{A1}$$

$$Y_\ell^{-m} = \sin m\varphi \, \check{P}_\ell^m(\cos\vartheta), \quad 1 \le m \le \ell, \tag{A2}$$

and the functions $\check{P}_\ell^m(\mu)$ are given by

$$\check{P}_\ell^m(\mu) = \begin{cases} \sqrt{2\frac{(\ell-m)!}{(\ell+m)!}}\, P_\ell^m(\mu) & \text{if } 1 \le m \le \ell \\ P_\ell(\mu) & \text{if } m = 0, \end{cases} \tag{A3}$$

where $P_\ell^m(\mu)$ are the associated Legendre functions [*Backus et al.*, 1996, equation (3.7.2)].

Appendix B: Intermediate Steps Between Equations (8) and (9)

Here the equivalence of (8) and (9) is shown by going backward from (9) to (8):

$$\nabla(\mathbf{u}\cdot\mathbf{A}) = (\mathbf{u}\cdot\nabla)\mathbf{A} + \underbrace{(\mathbf{A}\cdot\nabla)\mathbf{u} + \mathbf{A}\times(\nabla\times\mathbf{u})}_{\alpha} + \mathbf{u}\times(\nabla\times\mathbf{A}) \tag{B1}$$

$$\alpha = (\mathbf{A}\cdot\nabla)(\boldsymbol{\Omega}\times\mathbf{r}) + \mathbf{A}\times(\nabla\times(\boldsymbol{\Omega}\times\mathbf{r}) \tag{B2}$$

$$= (A_x\partial_x + A_y\partial_y + A_z\partial_z)(-\Omega y\hat{\boldsymbol{x}} + \Omega x\hat{\boldsymbol{y}}) + \mathbf{A}\times(2\boldsymbol{\Omega}) \tag{B3}$$

$$= \boldsymbol{\Omega}\times\mathbf{A} + 2\mathbf{A}\times\boldsymbol{\Omega} = \mathbf{A}\times\boldsymbol{\Omega}. \tag{B4}$$

Filling (B4) into (B1) gives

$$\nabla(\mathbf{u}\cdot\mathbf{A}) = (\mathbf{u}\cdot\nabla)\mathbf{A} - \boldsymbol{\Omega}\times\mathbf{A} + \mathbf{u}\times(\nabla\times\mathbf{A}). \tag{B5}$$

Appendix C: Intermediate Steps Between Equations (17) and (18)

Starting from equation (17), the term $\sin\vartheta\partial_\vartheta Y_\ell^m$ has to be expressed in spherical harmonics. With Schmidt seminormalized harmonics we have

$$\sin\vartheta\partial_\vartheta Y_\ell^m = -\frac{\ell+1}{2\ell+1}\sqrt{(\ell+m)(\ell-m)}Y_{\ell-1}^m + \frac{\ell}{2\ell+1}\sqrt{(\ell+m+1)(\ell-m+1)}Y_{\ell+1}^m. \tag{C1}$$

Inserting this into (17) gives

$$\begin{aligned}\Phi'_\omega(\mathbf{r}) = \sum_{\ell=1}^{\infty}\sum_{m=-\ell}^{\ell}\frac{\Omega r a}{\ell}\left(\frac{a}{r}\right)^{\ell+1} g_\ell^m\Bigg[-\frac{\ell+1}{2\ell+1}\sqrt{(\ell+m)(\ell-m)}Y_{\ell-1}^m(\vartheta,\varphi)\\ +\frac{\ell}{2\ell+1}\sqrt{(\ell+m+1)(\ell-m+1)}Y_{\ell+1}^m(\vartheta,\varphi)\Bigg],\end{aligned} \tag{C2}$$

which now has to be reordered. Substituting $\ell' = \ell - 1$ in the first term and $\ell' = \ell + 1$ in the second term and regrouping yields

$$\begin{aligned}\Phi'_\omega(\mathbf{r}) = \sum_{\ell'=1}^{\infty}\sum_{m=-\ell'}^{\ell'}\Bigg[-\frac{\Omega r a}{\ell'+1}\left(\frac{a}{r}\right)^{\ell'+2} g_{\ell'+1}^m\frac{\ell'+2}{2\ell'+3}\sqrt{(\ell'+m+1)(\ell'-m+1)}\\ +\frac{\Omega r a}{\ell'-1}\left(\frac{a}{r}\right)^{\ell'} g_{\ell'-1}^m\frac{\ell'-1}{2\ell'-1}\sqrt{(\ell'+m)(\ell'-m)}\Bigg]Y_{\ell'}^m(\vartheta,\varphi),\end{aligned} \tag{C3}$$

which can be rewritten as in (18).

Appendix D: Derivation of the Corotation Charge Density

The corotation charge density is derived from the Laplacian of the corotation potenial of equation (18) as

$$\rho = \epsilon_0\nabla^2\Phi'_\omega. \tag{D1}$$

Using (28) and (30) then gives

$$\rho = \frac{\epsilon_0}{r^2}\left(\partial_r r^2\partial_r + \nabla_s^2\right)\Phi'_\omega \tag{D2}$$

$$= \frac{\epsilon_0\Omega}{r^2}\sum_{\ell=0}^{\infty}\sum_{m=-\ell}^{\ell}\left(\partial_r r^2\partial_r - \ell(\ell+1)\right)\left(\frac{a}{r}\right)^{\ell+1} f_\ell^m(r)Y_\ell^m(\vartheta,\varphi) \tag{D3}$$

$$= \frac{\epsilon_0\Omega}{r^2}\sum_{\ell=0}^{\infty}\sum_{m=-\ell}^{\ell}a^{\ell+1}\left(-\frac{2\ell}{r^\ell}\partial_r f_\ell^m(r) + \frac{1}{r^{\ell-1}}\partial_r^2 f_\ell^m(r)\right)Y_\ell^m(\vartheta,\varphi). \tag{D4}$$

Considering that

$$\partial_r f_\ell^m(r) = 2r\frac{\sqrt{(\ell+m)(\ell-m)}}{2\ell-1}g_{\ell-1}^m \tag{D5}$$

$$\partial_r^2 f_\ell^m(r) = 2\frac{\sqrt{(\ell+m)(\ell-m)}}{2\ell-1}g_{\ell-1}^m \tag{D6}$$

gives

$$\rho = \frac{\epsilon_0\Omega}{r^2}\sum_{\ell=0}^{\infty}\sum_{m=-\ell}^{\ell} a^{\ell+1}(2-4\ell)\frac{\sqrt{(\ell+m)(\ell-m)}}{r^{\ell-1}(2\ell-1)}g_{\ell-1}^m Y_\ell^m(\vartheta,\varphi) \tag{D7}$$

$$= -2\epsilon_0\Omega\sum_{\ell=2}^{\infty}\sum_{m=-\ell}^{\ell}\sqrt{(\ell+m)(\ell-m)}\left(\frac{a}{r}\right)^{\ell+1} g_{\ell-1}^m Y_\ell^m(\vartheta,\varphi) \tag{D8}$$

consistent with equation (31).

Acknowledgments
Helpful comments and suggestions by Gauthier Hulot, Art Richmond, Hermann Lühr, Frank Lowes, Mikhail Kruglyakov, and Donald Melrose are gratefully acknowledged. The satellite data used for this study were kindly provided free of cost by the Swarm team of the European Space Agency. For Swarm data access see https://earth.esa.int/web/guest/swarm/data-access. The POMME10 geomagnetic model and software used for this study is freely available for download at http://geomag.org/models/pomme10.html. This work was supported by NASA grant NNX13AL20G.

References

Backus, G. (1956), The external magnetic field of a rotating magnet, *Astrophys. J.*, *123*, 508–512.
Backus, G. (1986), Poloidal and toroidal fields in geomagnetic field modeling, *Rev. Geophys.*, *24*, 75–109.
Backus, G., R. L. Parker, and C. Constable (1996), *Foundations of Geomagnetism*, Cambridge Univ. Press, Cambridge, U. K.
Baumjohann, W., and R. Treumann (1997), *Basic Space Plasma Physics*, Imperial College Press, London.
Burch, J. L., J. Goldstein, and B. R. Sandel (2004), Cause of plasmasphere corotation lag, *Geophys. Res. Lett.*, *31*, L05802, doi:10.1029/2003GL019164.
Coley, W. R., R. A. Heelis, and M. R. Hairston (2006), Characteristics of high-latitude vertical plasma flow from the Defense Meteorological Satellite Program, *J. Geophys. Res.*, *111*, A11314, doi:10.1029/2005JA011553.
Davis, L. (1947), Stellar electromagnetic fields, *Phys. Rev.*, *72*, 632.
Dumin, Y. V. (2002), The corotation field in collisionless magnetospheric plasma and its influence on average electric field in the lower atmosphere, *Adv. Space Res.*, *30*, 2209–2214, doi:10.1016/S0273-1177(02)80224-1.
Friis-Christensen, E., H. Lühr, and G. Hulot (2006), Swarm: A constellation to study the Earth's magnetic field, *Earth Planets Space*, *58*, 351–358, doi:10.1186/BF03351933.
Hones, E. W., and J. E. Bergeson (1965), Electric field generated by a rotating magnetized sphere, *J. Geophys. Res.*, *70*, 4951–4958.
Irvine, W. M. (1964), Electrodynamics in a rotating system of reference, *Physica*, *30*, 1160–1170.
Kennard, E. H. (1912), Unipolar induction, *Phil. Mag.*, *23*, 937–942.
Lejosne, S., and J. G. Roederer (2016), The zebra stripes: An effect of *F* region zonal plasma drifts on the longitudinal distribution of radiation belt particles, *J. Geophys. Res. Space Physics*, *121*, 507–518, doi:10.1002/2015JA021925.
Maus, S., and H. Lühr (2005), Signature of the quiet-time magnetospheric magnetic field and its electromagnetic induction in the rotating Earth, *Geophys. J. Int.*, *162*, 755–763, doi:10.1111/j.1365-246X.2005.02691.x.
Maus, S., H. Lühr, G. Balasis, M. Rother, and M. Mandea (2005), Potsdam magnetic model of the Earth, in *Earth Observation With CHAMP: Results From Three Years in Orbit*, edited by C. Reigber et al., pp. 293–298, Springer, Berlin.
Maus, S., C. Manoj, J. Rauberg, I. Michaelis, and H. Lühr (2010), NOAA/NGDC candidate models for the 11th generation international geomagnetic reference field and the concurrent release of the 6th generation POMME magnetic model, *Earth Planets Space*, *62*(10), 729–735, doi:10.5047/eps.2010.07.006.
McIlwain, C. E. (1961), Coordinates for mapping the distribution of magnetically trapped particles, *J. Geophys. Res.*, *66*(11), 3681–3691, doi:10.1029/JZ066i011p03681.
Melrose, D. B. (1967), Rotational effects on the distribution of thermal plasma in the magnetosphere of Jupiter, *Planet. Space Sci.*, *15*, 381–393, doi:10.1016/0032-0633(67)90202-4.
Melrose, D. B., and R. Yuen (2012), Obliquely rotating pulsars: Screening of the inductive electric field, *Astrophys. J.*, *745*, 169, doi:10.1088/0004-637X/745/2/169.
Melrose, D. B., and R. Yuen (2016), Pulsar electrodynamics: An unsolved problem, *J. Plasma Phys.*, *82*(2), 635820202, doi:10.1017/S0022377816000398.
Mozer, F. S. (1973), Electric fields and plasma convection in the plasmasphere, *Rev. Geophys.*, *11*(3), 755–765.
Olsen, N., H. Lühr, T. J. Sabaka, M. Mandea, M. Rother, L. Tøffner-Clausen, and S. Choi (2006), CHAOS—A model of Earth's magnetic field derived from CHAMP: Ørsted, and SAC-C magnetic satellite data, *Geophys. J. Int.*, *166*, 67–75, doi:10.1111/j.1365-246X.2006.02959.x.
Olsen, N., et al. (2015), The Swarm initial field model for the 2014 geomagnetic field, *Geophys. Res. Lett.*, *42*, 1092–1098, doi:10.1002/2014GL062659.
Redmon, R. J., W. K. Peterson, L. Andersson, E. A. Kihn, W. F. Denig, M. Hairston, and R. Coley (2010), Vertical thermal O+ flows at 850 km in dynamic auroral boundary coordinates, *J. Geophys. Res.*, *115*, A00J08, doi:10.1029/2010JA015589.
Reigber, C., H. Lühr, and P. Schwintzer (2002), CHAMP mission status, *Adv. Space Res.*, *30*, 129–134.
Rothwell, P. L. (2003), The superposition of rotating and stationary magnetic sources: Implications for the auroral region, *Phys. Plasmas*, *10*, 2971–2977, doi:10.1063/1.1582473.
Rothwell, P. L. (2004), Response to "Comment on "The superposition of rotating and stationary magnetic sources: Implications for the auroral region"" [Phys. Plasmas 11, 1738 (2004)], *Phys. Plasmas*, *11*, 1740–1743, doi:10.1063/1.1667493.
Ruderman, M. A., and P. G. Sutherland (1975), Theory of pulsars—Polar caps, sparks, and coherent microwave radiation, *Astrophys. J.*, *196*, 51–72, doi:10.1086/153393.
Sandel, B., J. Goldstein, D. Gallagher, and M. Spasojevic (2003), Extreme ultraviolet imager observations of the structure and dynamics of the plasmasphere, *Space Sci. Rev.*, *109*(1), 25–46, doi:10.1023/B:SPAC.0000007511.47727.5b.
Synge, J. L. (1960), *Relativity: The General Theory*, North Holland Publ., Colo.

Thomsen, P., and F. Hansen (1999), Danish Ørsted mission in-orbit experiences and status of the Danish small satellite programme, *in Proceedings of the 13th Annual AIAA/USU Conference on Small Satellites, August 23–26*, SSC99-I-8, Utah State Univ., Logan, Utah.
Vasyliunas, V. M. (2004), Comment on "The superposition of rotating and stationary magnetic sources: Implications for the auroral region" [Phys. Plasmas 10, 2971 (2003)], *Phys. Plasmas*, *11*, 1738–1739, doi:10.1063/1.1667492.
Volland, H. (1985), *Atmospheric Electrodynamics (Physics and Chemistry in Space)*, vol. 11, Springer, Berlin.
Webster, D. L. (1963), Schiff's charges and currents in rotating matter, *Am. J. Phys.*, *31*, 590–597.
Yau, A. W., and M. André (1997), Sources of ion outflow in the high latitude ionosphere, *Space Sci. Rev.*, *80*, 1–25.

Erratum

In the originally published version of this article, it was assumed that the drift of the plasma was caused by the electric field alone. However, there is actually a further effect called "Fermi acceleration" that should be taken into account. When bouncing back and forth along a geomagnetic field line in the plasmasphere, a charged particle is alternately accelerated at the westward mirror point and decelerated at the eastward mirror point. Consequently, the particle's kinetic energy as seen in the rest frame is slightly greater when its motion is in the direction of Earth rotation than when it is in the opposite direction. As confirmed by particle trajectory simulations in the inertial frame, this additional acceleration exactly compensates for the underrotation predicted from the corotation electric field alone. Therefore, one of the original conclusions of the paper is incorrect – that the nonaxially symmetric contributions of the geomagnetic field are found to slow down the corotation of the plasmasphere. This conclusion has since been removed from the Abstract, Introduction, Results and Discussion sections of the paper, and it has been clarified that observations of plasmasphere underrotation must be due to other effects. This updated version may be considered the authoritative version of record.